

Supporting Information for

Influence of the UV/H₂O₂ Advanced Oxidation Process on Dissolved Organic Matter and the Connection between Elemental Composition and Disinfection Byproduct Formation

Yingying Xiang,[†] Michael Gonsior,[‡] Philippe Schmitt-Kopplin,^{§,||} and Chii Shang^{*,†,⊥}

[†]Department of Civil and Environmental Engineering, The Hong Kong University of Science and Technology, Clear Water Bay, Kowloon 000, Hong Kong SAR

[‡]Chesapeake Biological Laboratory, University of Maryland Center for Environmental Science, Solomons, Maryland 20688, United States

[§]Helmholtz Zentrum Muenchen, Research Unit Analytical BioGeoChemistry, Neuherberg 85764, Germany

^{||}Technische Universität München, Chair of Analytical Food Chemistry, Freising-Weihenstephan 80333, Germany

[⊥]Hong Kong Branch of Chinese National Engineering Research Center for Control & Treatment of Heavy Metal Pollution, The Hong Kong University of Science and Technology, Clear Water Bay, Kowloon 000, Hong Kong SAR

* C. Shang. E-mail: cechii@ust.hk. Tel: +852 2358 7885.

Table of contents

Text S1 Details of materials and methods	5
Text S2 Effect of chlorine as the quenching agent of H ₂ O ₂ on the TOCl level.....	8
Text S3 Mass difference network analysis	8
Text S4 Definition of a significant increase or decrease in FT-ICR-MS peak intensity	9
Text S5 Determination of the required HO• exposure to degrade 90% of CBZ	10
Text S6 Calculation of the changes in total intensity of organic chlorine detected by FT-ICR-MS ...	11
Text S7 The expression of the boundaries of Zone 1, 2 and 3 in Fig. 4e and 4f.....	11
Text S8 The expression of the boundaries of Zone 1, 2 and 3 in Fig. S10c and S10d.....	12
Text S9 Effects of other water constituents on AOPs in alteration of the DBP formation from LHDOM.	13
Figure S1. The formation of TOCl after 3-day chlorination of SRNOM, SRNOM spiked with H ₂ O ₂ , and AOP-treated SRNOM. Conditions: [SRNOM] ₀ = 3 mg/L as C, [H ₂ O ₂] ₀ = 10 mg/L, [3-day residual free chlorine] = 1 ± 0.5 mg/L as Cl ₂ , [UV fluence] = 800 mJ cm ⁻² , pH = 7.....	14
Figure S2. UV fluence-dependent CBZ degradation by the UV/H ₂ O ₂ AOP. Conditions: [CBZ] ₀ = 2 μM, [SRNOM] ₀ = 3 mg/L as C, [H ₂ O ₂] ₀ = 10 mg/L, pH = 7.	14
Figure S3. UPLC/Orbitrap-MS/MS SIM (<i>m/z</i> 230.902) chromatograms of (a) 2,6-dihydroxybenzoic acid and (b) DOM treated by the UV/H ₂ O ₂ AOP followed by 3-d chlorination; UPLC/Orbitrap-MS/MS product ion scan spectra (<i>m/z</i> 230.902, RT = 3.5 min) of (c) 2,6-dihydroxybenzoic acid and (d) DOM treated by the UV/H ₂ O ₂ AOP followed by 3-d chlorination; (e) Possible structures of C ₅ H ₃ O ₄ Cl ₃ (<i>m/z</i> 230.902).	15
Figure S4. Mass difference network analysis of C ₁₆ H _n O _m and C ₁₆ H _n O _m Cl _x detected in SRNOM, SRNOM-AOP, 3-day chlorination of SRNOM and 3-day chlorination of SRNOM-AOP.....	16
Figure S5. The van Krevelen space was divided into three zones based on the possibility of the C ₇₋₂₂ H _n O _m formulas located in each zone to match with their corresponding DBPs. (i.e., Zone 1: precursors, Zone 2: possible precursors, and Zone 3: non-precursors)	17
Figure S6. Van Krevelen diagrams of C ₇₋₂₂ H _n O _m formulas in SRNOM and SRNOM-AOP. The formulas were classified as (a)–(b) DBP precursors and (c)–(d) non-precursors by considering chlorine substitution as the transformation pathway.....	18
Figure S7. Van Krevelen diagrams of C ₇₋₂₂ H _n O _m formulas in SRNOM and SRNOM-AOP. The formulas were classified as (a)–(b) DBP precursors and (c)–(d) non-precursors by considering HOCl addition as the transformation pathway.	19
Figure S8. Van Krevelen diagrams of LHDOM and SRNOM. The areas of bubbles reflect the relative	

intensities of each formula.	20
Figure S9. Van Krevelen diagrams of the chlorinated DBPs produced after 3-day chlorination of LHDOM and SRNOM. The areas of bubbles reflect the relative intensities of each formula.	20
Figure S10. (a) Van Krevelen diagram of CHO formulas in LHDOM and LHDOM-AOP. (b) AI_{mod} diagram of chlorinated DBPs produced during 3-day chlorination of LHDOM and LHDOM-AOP. (c)–(d) The three zones of LHDOM in the van Krevelen space were identified based on the possibility of the $C_{9-16}H_nO_m$ formulas located in each zone to match with their corresponding DBPs. The areas of bubbles reflect the relative intensities of each formula.	21
Figure S11. Van Krevelen diagrams of $C_{9-16}H_nO_m$ formulas in LHDOM and LHDOM-AOP. The formulas were classified as (a)–(b) DBP precursors and (c)–(d) non-precursors. Two chlorination pathways, chlorine substitution and HOCl addition, were considered. (e)–(f) The van Krevelen space was divided into three zones based on the possibility of the $C_{9-16}H_nO_m$ formulas located in each zone to match with their corresponding DBPs. Note that the diagrams only covered $C_{9-16}H_nO_m$ formulas in LHDOM because the carbon number of the DBPs detected mainly ranges from 9–16.	22
Figure S12. ESI-tqMS precursor ion scan spectra of (a) m/z 35 and (b) m/z 37 of 1,2,4,5-benzenetetracarboxylic acid treated by 3-day chlorination.	24
Figure S13. High-resolution mass spectrometry full scan spectra of the chlorine-containing products generated from 1,2,4,5-benzenetetracarboxylic acid treated by the UV/ H_2O_2 AOP followed by 3-d chlorination. Isotope peaks of (a) m/z 258.9650 $C_9H_5O_7Cl$; (b) m/z 214.9747 $C_8H_5O_5Cl$; (c) m/z 170.9849 $C_7H_5O_3Cl$; (d) m/z 126.9954 C_6H_5OCl	25
Figure S14. High-resolution mass spectrometry full scan spectra of 2,6-dihydroxybenzoic acid after (a) the 3-d chlorination and (b) the UV/ H_2O_2 AOP followed by 3-d chlorination.	26
Figure S15. High-resolution mass spectrometry product ion scan spectra of the chlorine-containing products generated from 2,6-dihydroxybenzoic acid treated by the UV/ H_2O_2 AOP followed by 3-d chlorination. Product ion scan spectra of (a) m/z 220.9408 $C_7H_4O_4^{35}Cl_2$; (b) m/z 222.9381 $C_7H_4O_4^{35}Cl^{37}Cl$; (c) m/z 186.9798 $C_7H_5O_4^{35}Cl$ and (d) m/z 188.9769 $C_7H_5O_4^{37}Cl$	27
Figure S16. High-resolution mass spectrometry product ion scan spectra of the chlorine-containing products generated from 2,6-dihydroxybenzoic acid treated by the UV/ H_2O_2 AOP followed by 3-d chlorination. (a) m/z 176.9510 $C_6H_4O_2^{35}Cl_2$; (b) m/z 178.9481 $C_6H_4O_2^{35}Cl^{37}Cl$; (c) m/z 142.9900 $C_6H_5O_2^{35}Cl$ and (d) m/z 144.9870 $C_6H_5O_2^{37}Cl$	28
Figure S17. (a) Van Krevelen diagram and (b) modified Kendrick plots of $CHOCl$ and $CHOBr$ DBPs produced during 3-day chlorination of AOP-treated LHDOM in the presence and in the absence of water constituents.	29
Table S1 Summary of weighted mean values of O/C, H/C, DBE/C and AI_{mod} of formulas in SRNOM and SRNOM-AOP.	29

Table S2 Number and ratio of DBPs that can find the precursors in SRNOM vs. SRNOM-AOP (C_{7-22} represents the range of the carbon number of DBPs)	30
Table S3 Summary of weighted mean values of O/C, H/C, DBE/C and AI_{mod} of formulas in LHDOM and LHDOM-AOP.	30
Table S4 List of products detected by high-resolution mass spectrometry.	31
Table S5 Concentrations of water constituents	32
References:	32

Text S1 Details of materials and methods

Chemicals and Solutions

Solutions were prepared from reagent-grade chemicals with 18.2 M Ω -cm deionized water produced from a water purification system (Cascada, PALL Corporation). Carbamazepine (CBZ), 1,2,4,5-benzenetetracarboxylic acid (1,2,4,5-BTetraCA), 2,6-dihydroxybenzoic acid (2,6-DHBA), sodium hypochlorite solution (NaClO), H₂O₂ and sodium thiosulfate (Na₂S₂O₃) were purchased from Sigma-Aldrich. Methanol of HPLC grade was purchased from Fisher Scientific. Methanol of mass spectrometry grade was purchased from J.T. Baker. Water containing 0.1% (v/v) formic acid of mass spectrometry grade was purchased from Sigma-Aldrich. DOM stock solutions (about 300 mg/L as C) were prepared by dissolving SRNOM or LHDOM in deionized water and filtered through 0.45 μ m membrane filters and stored at 4 °C. A H₂O₂ stock solution (about 280 mM) was diluted from the 30% H₂O₂ solution. A free chlorine stock solution (about 2500 mg/L as Cl₂) was prepared by diluting the 4% sodium hypochlorite (NaClO) solution and periodically standardized by DPD/FAS titration.

Experimental Procedures

UV exposure was carried out in a 700 mL cylindrical photoreactor equipped with a low pressure (LP) UV lamp (Heraeus, GPH 212T5L/4, 10 W, 254 nm) in a quartz sleeve. Rapid mixing was provided at the bottom of the reactor. The LP UV lamp was warmed up for at least 30 min prior to the tests. Experiments were initiated by adding a H₂O₂ stock solution to the UV reactor containing a solution spiked with 3 mg/L C SRNOM or LHDOM to give a H₂O₂ concentration of 10 mg/L. The pH was adjusted to pH 7 by adding NaOH (0.1 M) or H₂SO₄ (0.1 M). After the UV/H₂O₂ AOP at a UV fluence of 800 mJ cm⁻², a 600 mL sample was collected, and chlorine was added to quench unreacted H₂O₂ and yield a 3-day residual free chlorine of 1 \pm 0.5 mg/L. The 3-day chlorination was conducted in a sealed glass bottle in the dark at room temperature. The sampling points included untreated DOM, DOM treated by 3-day chlorination, UV/H₂O₂-treated DOM and UV/H₂O₂-treated DOM followed by 3-day chlorination, and all tests were duplicated. The effect of chlorine as the quenching agent of H₂O₂ on the DBP level observed after the 3-day chlorination of AOP-treated DOM was evaluated and

detailed in Text S2 and Figure S1. The tests using model compounds (i.e., 1,2,4,5-BTetraCA and 2,6-DHBA) were conducted in a similar manner except that 3 mg/L as C of 1,2,4,5-BTetraCA or 2,6-DHBA, instead of DOM, was added. Text S5 and Figure S2 show the experimental procedure in the determination of the required HO• exposure to degrade 90% of CBZ at an environmental-related concentration (0.2 nM).

Tests measuring the regulated DBPs (i.e. THMs and HAAs) and TOCl formation potential of untreated DOM and the AOP-treated DOM were conducted using a similar approach as described above. After the UV/H₂O₂ AOP, a 600 mL sample was collected, and chlorine was added to quench unreacted H₂O₂ and to yield a 3-day free chlorine residual of 1 ± 0.5 mg/L. The 3-day chlorination was conducted in a sealed glass bottle in the dark at room temperature. For the measurement of THMs and HAAs, 20 mL and 10 mL samples, respectively, were collected and quenched with ascorbic acid, and then subjected to the pretreatment procedure for THM and HAA detection. For the TOCl measurement, 100 mL samples were collected and quenched with Na₂S₂O₃ and stored at 4 °C in the dark before the TOX measurement.

Analytical Methods

FT-ICR-MS

A 600 mL sample was collected and quenched by Na₂S₂O₃ and acidified to pH 2.5 using concentrated HCl. The acidified samples were extracted using Agilent Bond Elut PPL cartridges (500 mg resin) that were activated by 5 mL LCMS grade methanol and rinsed by 5 mL LCMS grade water (0.1% formic acid). A vacuum pump was applied and the sample flow rate through the cartridge was controlled at less than 10 mL/min. Before sample elution, the cartridge was rinsed by 10 mL of LCMS grade water (0.1% formic acid) to remove halides and other salts. Cartridges were dried with a vacuum pump and eluted with 5 mL LCMS grade methanol. The eluted samples were stored in pre-combusted amber glass vials at –36 °C prior to analysis. The recoveries of TOC and TOCl were $51 \pm 1\%$ and $43 \pm 4\%$, respectively.

The SRNOM samples were analyzed by using a Bruker Solarix 9.4 T FT-ICR-MS equipped with an

electrospray ionization (ESI) source (Bruker Daltonik GmbH, Bremen, Germany) at Guangzhou Institute of Geochemistry (Chinese Academy of Sciences, Guangzhou, China). The samples were ionized in negative ionization mode with an ion accumulation time of 0.7 s and the mass range was set to m/z 150–1200. The analysis of LHDOM samples was performed using a Bruker Solarix 12 T FT-ICR-MS at the Helmholtz Center for Environmental Science (Munich, Germany). The ion accumulation time was set to 0.3 s. A total of 300 continuous 4 megaword (M) data FT-ICR transients were averaged to enhance the signal-to-noise (S/N) ratio and dynamic range. External calibration of the spectrum was conducted with arginine clusters in negative ion mode. The spectrum was also internally recalibrated in DataAnalysis 4.4 (Bruker Daltonics). A mass-resolving power ($m/\Delta m_{50\%}$) of > 450 000 and a mass error of < 0.3 ppm at m/z 319 was achieved. All m/z ions were selected if the S/N was larger than 10, the specific intensity was higher than 1×10^6 and the relative intensity was higher than 0.0001%. The molecular formulas were automatically assigned by an in-house written software according to the criteria: $^{12}\text{C}_{0-78}$, $^{13}\text{C}_{0-2}$, $^{16}\text{O}_{0-27}$, $^{18}\text{O}_{0-1}$, $^1\text{H}_{0-126}$, $^{35}\text{Cl}_{0-5}$, $^{37}\text{Cl}_{0-5}$. Statistical analysis was applied, and the Bray–Curtis dissimilarity between replicates was calculated to be 2.42%, indicates an excellent reproducibility. The intensity changes of the common formula in different samples were compared using their absolute intensity. All Cl-containing formulas were verified by checking the similarity between measured and theoretical isotopic patterns, and the mass error between the theoretical and exact m/z values was within 0.5 ppm.

Heteroatoms including N, S and P comprised only 1.27%, 1.78% and ~0%, respectively, of the total mass of SRNOM (2R101N). It has been reported that only 152 CHOS formulas were detected in SRNOM by FT-ICR-MS, which contributed less than 5% of the total formulas assigned in SRNOM.¹ Our preliminary tests show that only three S-containing DBPs, including $\text{C}_4\text{H}_3\text{O}_4\text{S}_2\text{Cl}_3$, $\text{C}_4\text{H}_4\text{O}_4\text{S}_2\text{Cl}_4$ and $\text{C}_5\text{H}_3\text{O}_6\text{S}_2\text{Cl}_3$, were detected at very low intensity by FT-ICR-MS in the SRNOM sample after 3-day chlorination. Due to their presence at small quantity in the precursor and DBPs, the heteroatoms were not included in the analysis.

Mass Difference Network Analysis

The possible transformation networks from precursors to DBPs were calculated by functional network reconstruction and visualized by Gephi software. The basis of the mass difference network analysis is detailed in SI Text S3. Theoretical masses of all CHO formulas were considered as reference masses. Formulas will be connected if the mass differences between them were equal to the theoretical masses of O (15.994915 amu), H₂ (2.015650 amu), HOCl (51.971593 amu) and ClH₋₁ (33.961028 amu).

Other Analytical Methods

The concentration of CBZ was measured using an HPLC system (VP series, Shimadzu) equipped with a Waters symmetry C18 column (4.6 mm × 150 mm, 5 μm particle size) and a UV detector set at 268 nm. The transformation products of model compounds were identified with a Waters Synapt G2-Si Ion Mobility-Q-TOF high-resolution LC-MS device equipped with an HSS T3 column (100 × 2.1 mm, 1.8 μm particle size, Waters). The structural analyses of highly abundant unknown DBPs were conducted using a Thermo LTQ Orbitrap XL mass spectrometer.

Text S2 Effect of chlorine as the quenching agent of H₂O₂ on the TOCl level

A control test was conducted to evaluate the effect of chlorine as the quenching agent of H₂O₂ on the TOCl level observed after the AOP. In the absence of UV irradiation, H₂O₂ was spiked into the SRNOM solution and free chlorine was then added to yield a 3-day residual free chlorine of 1 ± 0.5 mg/L as Cl₂. As shown in Fig. S1, the TOCl concentration of the control group was 647 μg/L. The concentrations of TOCl after 3-day chlorination of SRNOM and AOP-treated SRNOM were 640 μg/L and 774 μg/L, respectively. Therefore, the influence of chlorine as the quencher of H₂O₂ was not significant on the TOCl level observed after the 3-day chlorination of AOP-treated SRNOM.

Text S3 Mass difference network analysis

During mass difference network analysis, the connections between formulas were assigned based on

their accurate mass differences. Taking $C_{12}H_6O_9Cl_2$ as an example, if chlorine substitution is the chlorination pathway, $C_{12}H_6O_9Cl_2$ should be formed by replacing a hydrogen atom of its precursor with a chlorine atom. Thus, the elemental difference between $C_{12}H_6O_9Cl_2$ and its precursor is $Cl_{+1}H_{-1}$, resulting in an accurate mass difference of 33.961028 amu. During the analysis, the accurate mass of the ions detected in the sample before and after chlorination is imported to an in-house written software. If the accurate mass difference between two ions in the list is found to be 33.961028 amu, the connection between them is identified as $Cl_{+1}H_{-1}$. On the other hand, if the accurate mass difference is calculated to be 51.971593 amu, the two ions are connected in the network by HOCl addition. In Fig.3, four mass differences, including 15.994915 amu (O), 2.015650 amu (H_2), 51.971593 amu (HOCl) and 33.961028 amu ($Cl_{+1}H_{-1}$), were used for searching the connections.

Text S4 Definition of a significant increase or decrease in FT-ICR-MS peak intensity

The percent deviation of peak intensity between replicates was calculated to define a significant increase or decrease in peak intensity between different samples. The intensity percent deviation of 95% of the peaks between replicates was found to be $\leq 19\%$. Therefore, an increase or a decrease of $\geq 20\%$ of the peak intensity between the same peaks in different samples was determined to be a significant difference.

Text S5 Determination of the required HO• exposure to degrade 90% of CBZ

The degradation of CBZ by the UV/H₂O₂ AOP was carried out in the 700 mL UV irradiation reactor described in the Experimental Procedures. The LP UV lamp was warmed up at least 30 min prior to the tests. Experiments were initiated by adding the H₂O₂ stock solution (10 ppm) to the UV reactor containing the solution spiked with 2 µM CBZ and 3 mg/L as C SRNOM to give an H₂O₂ concentration of 10 ppm. pH was controlled at pH 7 by adding phosphate buffer (2 mM). Samples (1 mL) were collected at different time intervals and quenched with Na₂S₂O₃ and stored at 4 °C in the dark before HPLC analysis.

A steady-state kinetic model modified according to a model established by Fang et al. was implemented with Kintecus (version 6.51).² The model was established based on the hypothesis that CBZ degradation in the UV/H₂O₂ AOP mainly attributed to HO•. A total of 41 reactions were considered in the model. The second-order rate constant of the reaction between DOM and HO• was set to $3 \times 10^8 \text{ M}^{-1} \text{ s}^{-1}$. As shown in Figure S2, the CBZ degradation (2 µM) simulated by the model fitted with the experimental data well. By changing the initial CBZ concentration to an environmental-related concentration (0.2 nM), the pseudo-first-order rate constant increased from $2.43 \times 10^{-3} \text{ cm}^2/\text{mJ}$ to $2.81 \times 10^{-3} \text{ cm}^2/\text{mJ}$, and the $[\text{HO}\bullet]_{\text{ss}}$ was determined to be $4.49 \pm 0.16 \times 10^{-13} \text{ M}$. The required UV fluence was calculated to be 800 mJ/cm² to achieve the 90% degradation of environmental-related concentration of CBZ.

Text S6 Calculation of the changes in total intensity of organic chlorine detected by FT-ICR-MS

The total absolute intensity of organic chlorine detected by FT-ICR-MS is calculated according to Eq.

1:

$$\text{Total absolute intensity of organic chlorine} = \sum_{k=1}^n I_k \cdot x_k \quad (1)$$

where I_k and x_k represent the absolute intensity and the number of chlorine atoms, respectively, of formula k. The total intensity of the 1495 DBPs detected in SRNOM-AOP followed with 3-day chlorination was calculated to be 69,752,845,173, and that of the 1477 DBPs detected in untreated DOM followed with 3-day chlorination was 58,429,451,196. Thus, the difference of the total intensity of organic chlorine detected by FT-ICR-MS between the untreated and AOP-treated samples was calculated to be $(69,752,845,173 - 58,429,451,196)/58,429,451,196 = 19.3\%$.

Text S7 The expression of the boundaries of Zone 1, 2 and 3 in Fig. 4e and 4f

Zone 1, 2 and 3 can be expressed as the areas in the ellipses.

Figure 4e:

$$\text{Zone 1:} \quad \sqrt{(x - 0.572)^2 + (y - 1.210)^2} + \sqrt{(x - 0.694)^2 + (y - 0.628)^2} \leq 0.661$$

$$\text{Zone 2:} \quad \sqrt{(x - 0.572)^2 + (y - 1.210)^2} + \sqrt{(x - 0.694)^2 + (y - 0.628)^2} > 0.661$$

$$\sqrt{(x - 0.526)^2 + (y - 1.380)^2} + \sqrt{(x - 0.638)^2 + (y - 0.610)^2} \leq 1.024$$

$$\text{Zone 3:} \quad \sqrt{(x - 0.526)^2 + (y - 1.380)^2} + \sqrt{(x - 0.638)^2 + (y - 0.610)^2} > 1.024$$

$$\sqrt{(x - 0.449)^2 + (y - 1.436)^2} + \sqrt{(x - 0.582)^2 + (y - 0.582)^2} \leq 1.242$$

Figure 4f:

$$\text{Zone 1: } \sqrt{(x - 0.479)^2 + (y - 1.123)^2} + \sqrt{(x - 0.601)^2 + (y - 0.552)^2} \leq 0.697$$

$$\text{Zone 2: } \sqrt{(x - 0.479)^2 + (y - 1.123)^2} + \sqrt{(x - 0.601)^2 + (y - 0.552)^2} > 0.697$$

$$\sqrt{(x - 0.472)^2 + (y - 1.271)^2} + \sqrt{(x - 0.615)^2 + (y - 0.477)^2} \leq 0.953$$

$$\text{Zone 3: } \sqrt{(x - 0.472)^2 + (y - 1.271)^2} + \sqrt{(x - 0.615)^2 + (y - 0.477)^2} > 0.953$$

$$\sqrt{(x - 0.449)^2 + (y - 1.436)^2} + \sqrt{(x - 0.582)^2 + (y - 0.582)^2} \leq 1.242$$

Text S8 The expression of the boundaries of Zone 1, 2 and 3 in Fig. S10c and S10d

Figure 5c:

$$\text{Zone 1: } \sqrt{(x - 0.57)^2 + (y - 1.49)^2} + \sqrt{(x - 0.70)^2 + (y - 0.75)^2} \leq 0.777$$

$$\text{Zone 2: } \sqrt{(x - 0.57)^2 + (y - 1.49)^2} + \sqrt{(x - 0.70)^2 + (y - 0.75)^2} > 0.777$$

$$\sqrt{(x - 0.51)^2 + (y - 1.65)^2} + \sqrt{(x - 0.72)^2 + (y - 0.64)^2} \leq 1.152$$

$$\text{Zone 3: } \sqrt{(x - 0.51)^2 + (y - 1.65)^2} + \sqrt{(x - 0.72)^2 + (y - 0.64)^2} > 1.152$$

$$\sqrt{(x - 0.48)^2 + (y - 1.91)^2} + \sqrt{(x - 0.70)^2 + (y - 0.40)^2} \leq 1.691$$

Figure 5d:

$$\text{Zone 1: } \sqrt{(x - 0.44)^2 + (y - 1.15)^2} + \sqrt{(x - 0.58)^2 + (y - 0.53)^2} \leq 0.676$$

$$\text{Zone 2: } \sqrt{(x - 0.44)^2 + (y - 1.15)^2} + \sqrt{(x - 0.58)^2 + (y - 0.53)^2} > 0.676$$

$$\sqrt{(x - 0.40)^2 + (y - 1.50)^2} + \sqrt{(x - 0.57)^2 + (y - 0.52)^2} \leq 1.073$$

Zone 3: $\sqrt{(x - 0.40)^2 + (y - 1.50)^2} + \sqrt{(x - 0.57)^2 + (y - 0.52)^2} > 1.073$

$$\sqrt{(x - 0.48)^2 + (y - 1.91)^2} + \sqrt{(x - 0.70)^2 + (y - 0.40)^2} \leq 1.691$$

Text S9 Effects of other water constituents on AOPs in alteration of the DBP formation from LHDOM.

In actual water in the drinking water treatment plants, there may exist other constituents that affect the AOPs in alteration of the DBP formation from DOM. Additional tests were conducted with the spikes of common water constituents, including HCO_3^- , HNO_3^- , SO_4^{2-} , Cl^- and Br^- , into the LHDOM solution at environmentally relevant concentrations (Table S5). After the UV/ H_2O_2 AOP followed by 3-day chlorination, 7 Br-containing unknown DBPs were detected in the LHDOM with the spikes of water constituents (Fig. S17). In addition, the total number of unknown DBPs detected by FT-ICR-MS decreased from 290 to 224 in the presence of the water constituents. This can be partially explained by the scavenging of $\text{HO}\cdot$ by HCO_3^- ($k = 8.5 \times 10^6 \text{ M}^{-1} \text{ s}^{-1}$), which inhibited the activation of LHDOM caused by hydroxylation during the AOP.

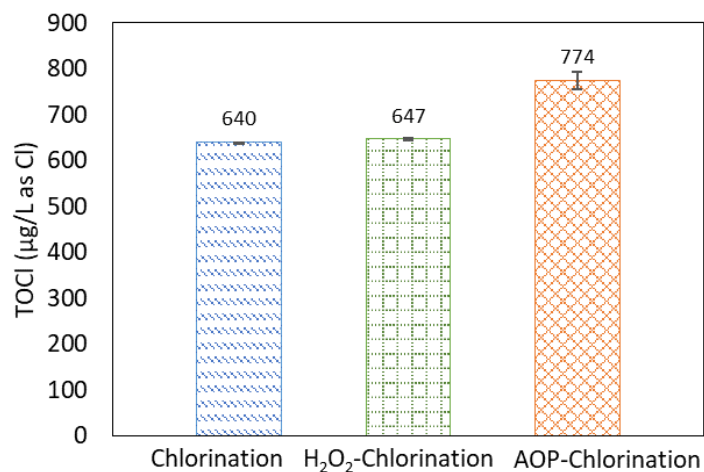


Figure S1. Formation of TOCl after 3-day chlorination of SRNOM, SRNOM spiked with H₂O₂, and AOP-treated SRNOM. Conditions: [SRNOM]₀ = 3 mg/L as C, [H₂O₂]₀ = 10 mg/L, [3-day residual free chlorine] = 1 ± 0.5 mg/L as Cl₂, [UV fluence] = 800 mJ cm⁻², pH = 7.

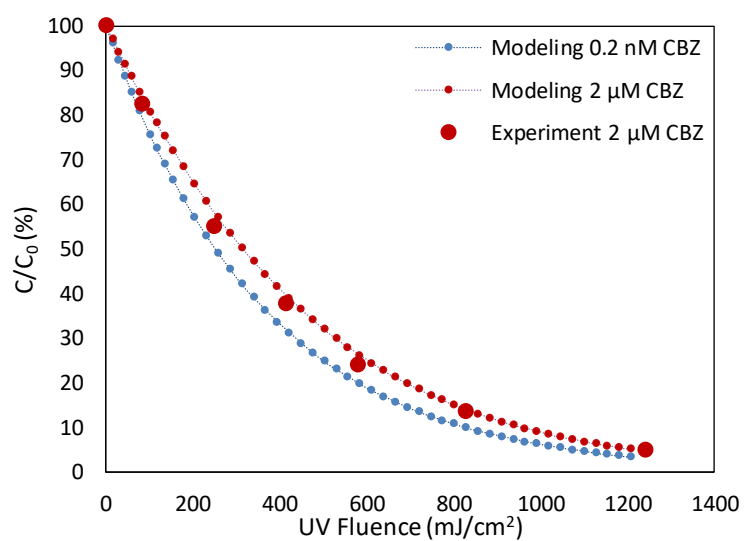


Figure S2. UV fluence-dependent CBZ degradation by the UV/H₂O₂ AOP. Conditions: [CBZ]₀ = 2 µM, [SRNOM]₀ = 3 mg/L as C, [H₂O₂]₀ = 10 mg/L, pH = 7.

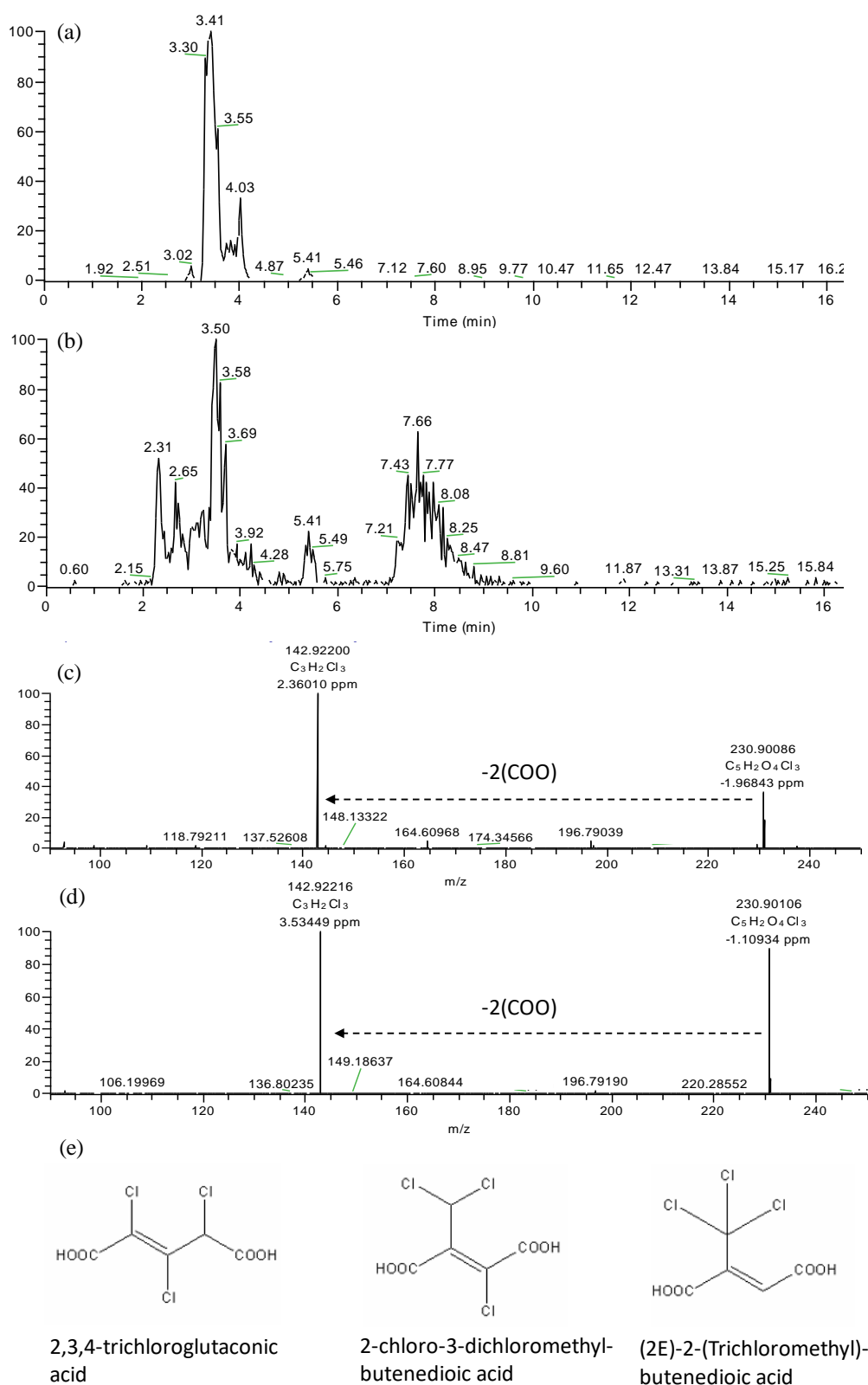


Figure S3. UPLC/Orbitrap-MS/MS SIM (m/z 230.902) chromatograms of (a) 2,6-dihydroxybenzoic acid and (b) DOM treated by the UV/ H_2O_2 AOP followed by 3-d chlorination; UPLC/Orbitrap-MS/MS

product ion scan spectra (m/z 230.902, RT = 3.5 min) of (c) 2,6-dihydroxybenzoic acid and (d) DOM treated by the UV/H₂O₂ AOP followed by 3-d chlorination; (e) Possible structures of C₅H₃O₄Cl₃ (m/z 230.902).

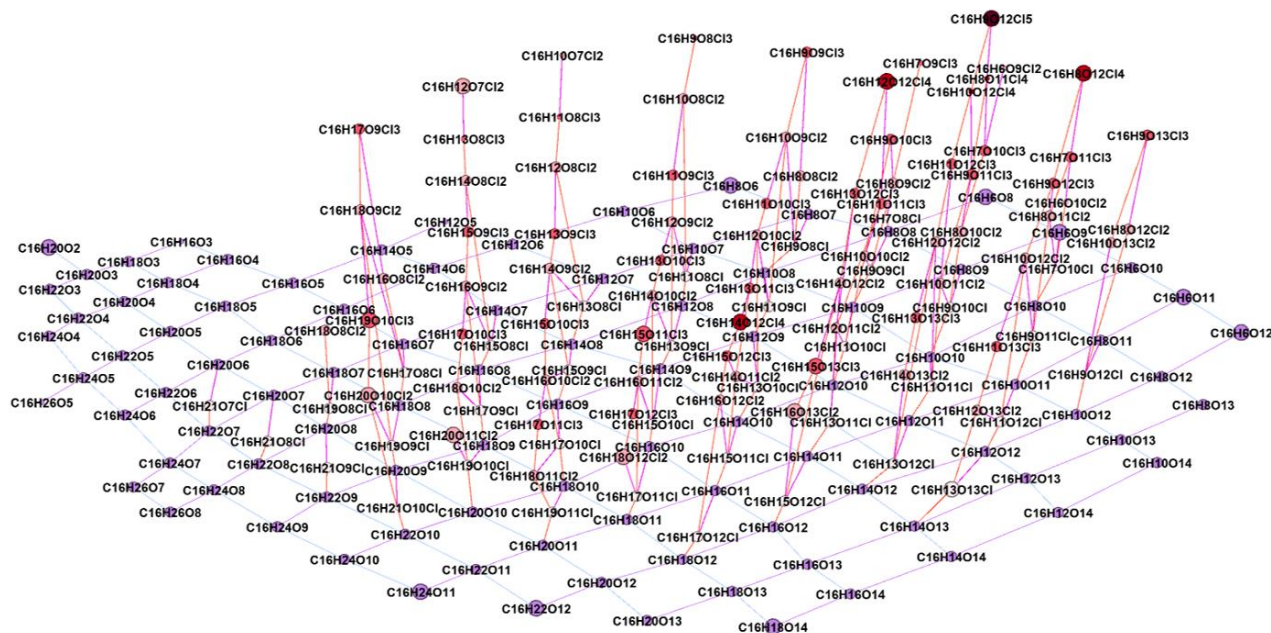


Figure S4. Mass difference network analysis of C₁₆H_nO_m and C₁₆H_nO_mCl_x detected in SRNOM, SRNOM-AOP, 3-day chlorination of SRNOM and 3-day chlorination of SRNOM-AOP.

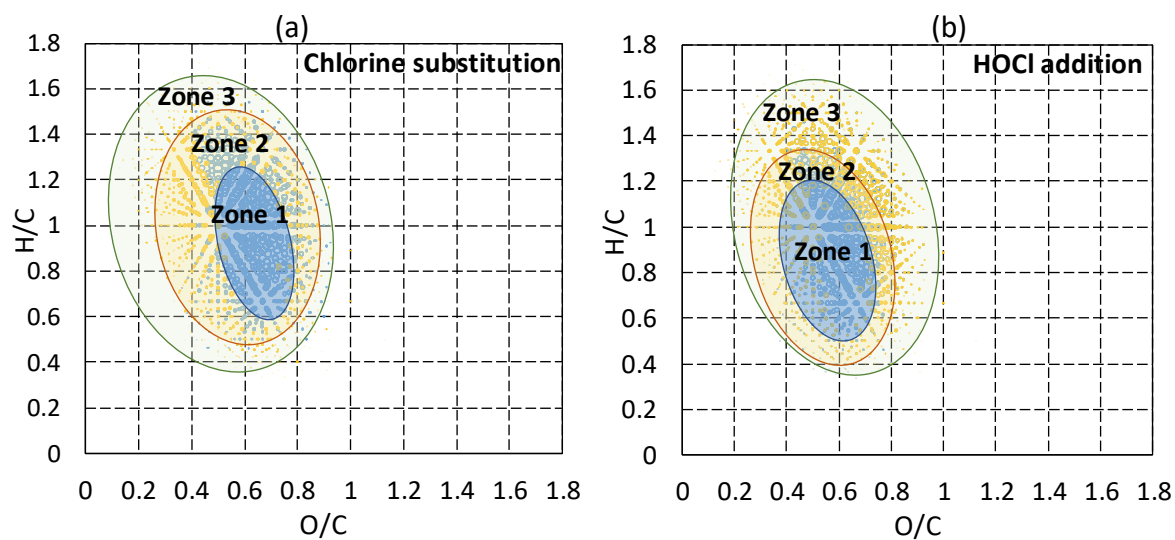


Figure S5. The van Krevelen space was divided into three zones based on the possibility of the C_7-
 $_{22}H_nO_m$ formulas located in each zone to match with their corresponding DBPs. (i.e., Zone 1:
 precursors, Zone 2: possible precursors, and Zone 3: non-precursors)

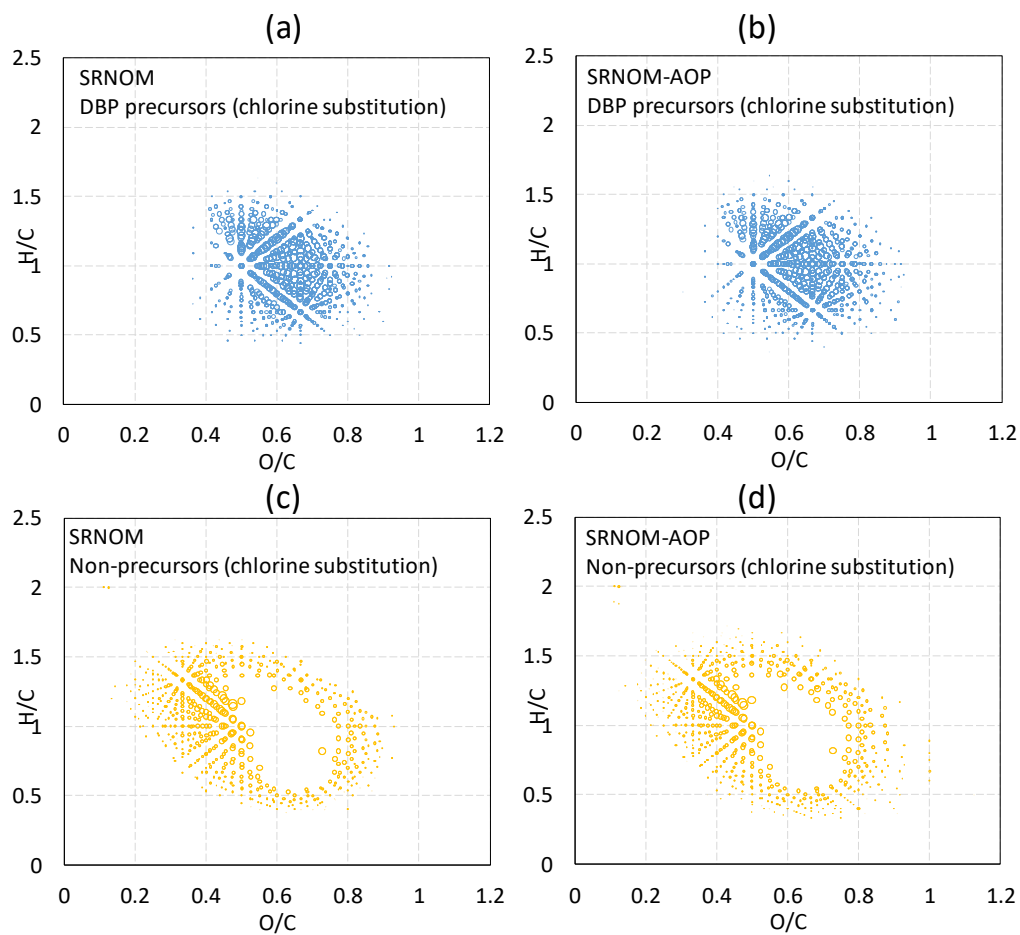


Figure S6. Van Krevelen diagrams of $C_{7-22}H_nO_m$ formulas in SRNOM and SRNOM-AOP. The formulas were classified as (a)–(b) DBP precursors and (c)–(d) non-precursors by considering chlorine substitution as the transformation pathway.

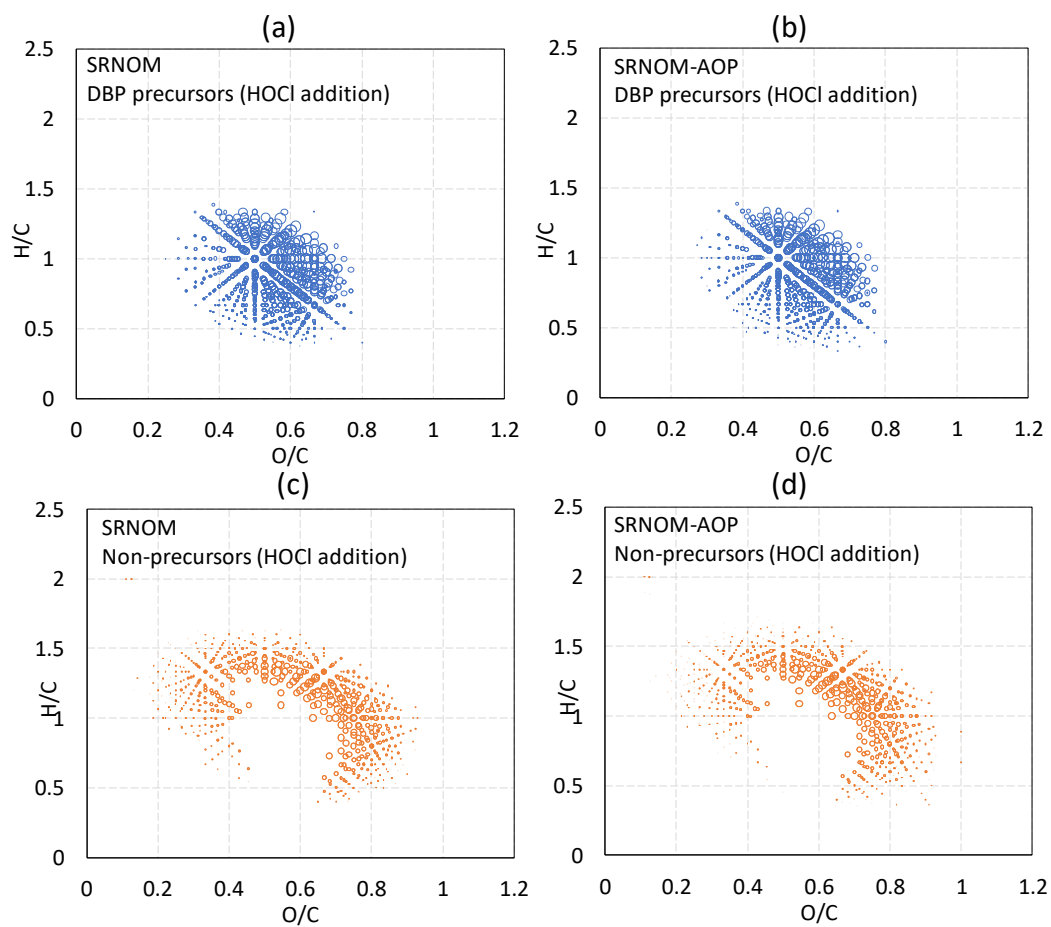


Figure S7. Van Krevelen diagrams of $C_{7-22}H_nO_m$ formulas in SRNOM and SRNOM-AOP. The formulas were classified as (a)–(b) DBP precursors and (c)–(d) non-precursors by considering HOCl addition as the transformation pathway.

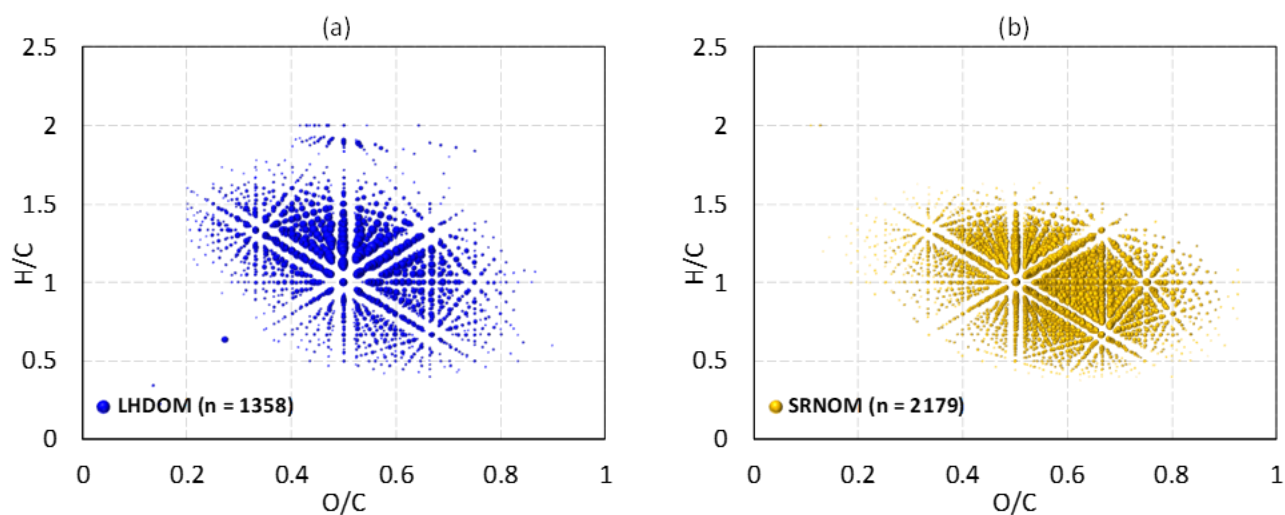


Figure S8. Van Krevelen diagrams of LHDOM and SRNOM. The areas of bubbles reflect the relative intensities of each formula.

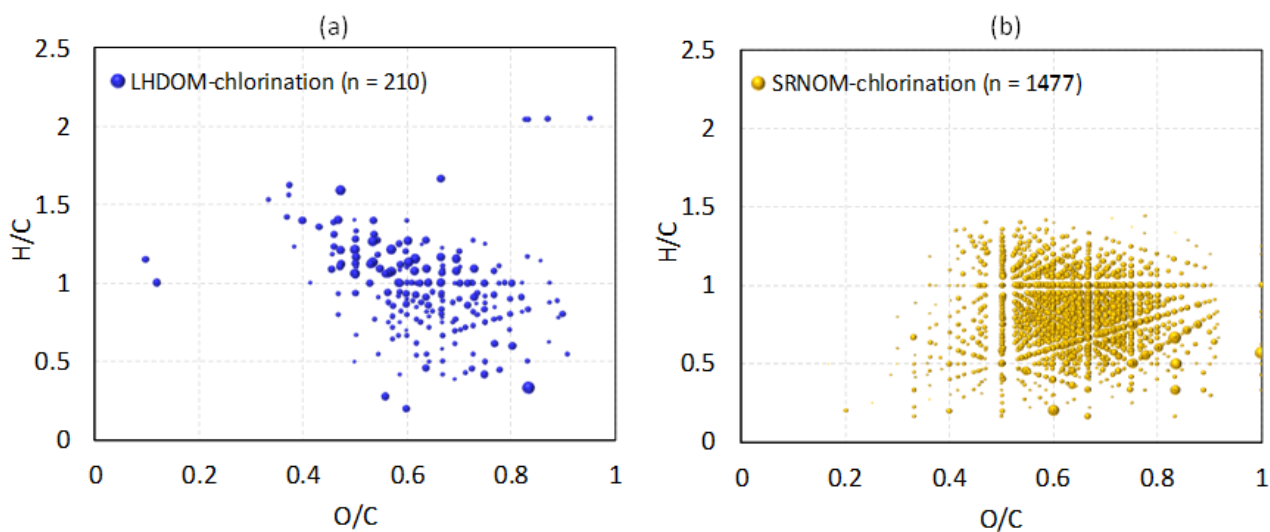


Figure S9. Van Krevelen diagrams of the chlorinated DBPs produced after 3-day chlorination of LHDOM and SRNOM. The areas of bubbles reflect the relative intensities of each formula.

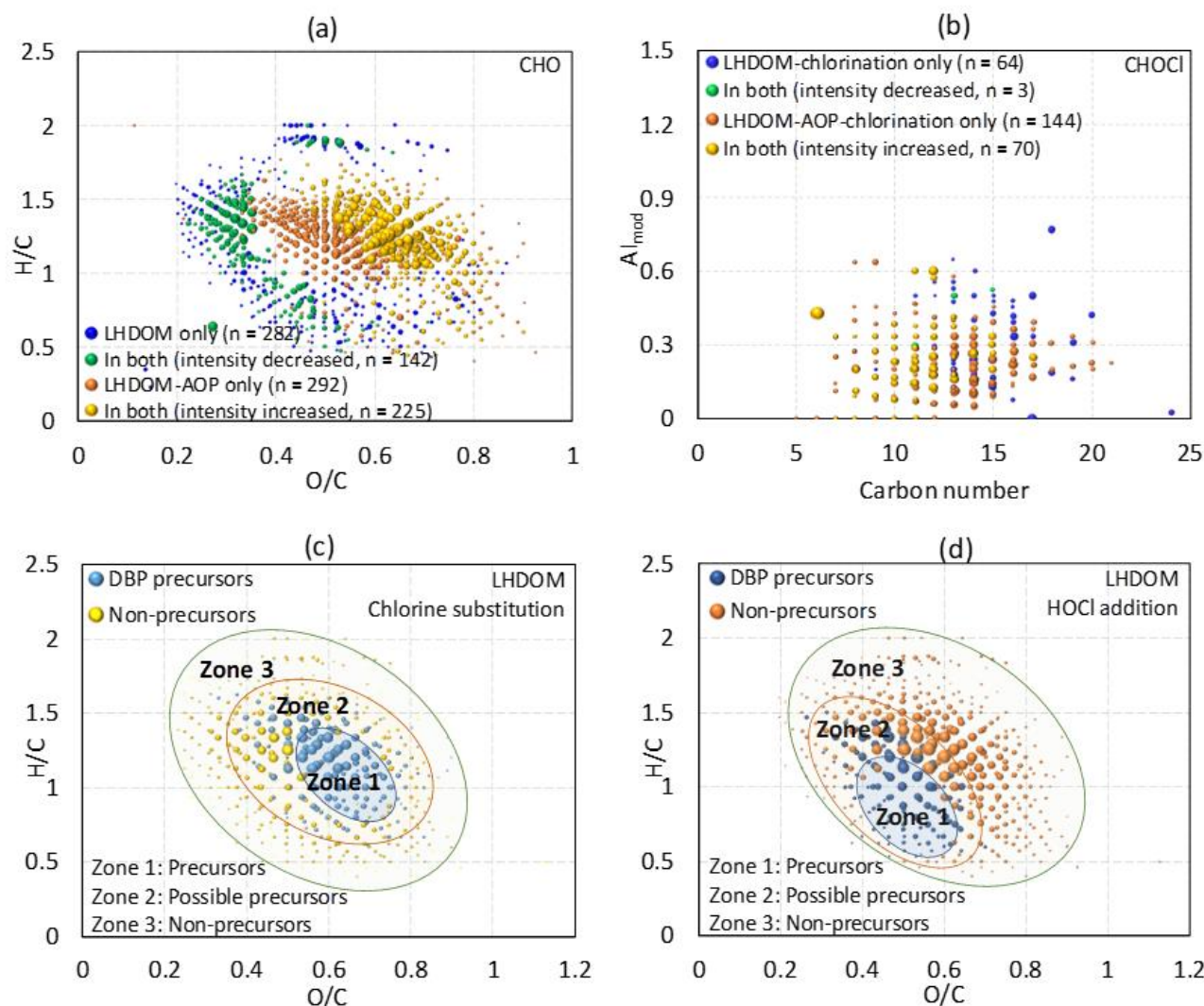


Figure S10. (a) Van Krevelen diagram of CHO formulas in LHDOM and LHDOM-AOP. (b) AI_{mod} diagram of chlorinated DBPs produced during 3-day chlorination of LHDOM and LHDOM-AOP. (c)–(d) The three zones of LHDOM in the van Krevelen space were identified based on the possibility of the $C_{9-16}H_nO_m$ formulas located in each zone to match with their corresponding DBPs. The areas of bubbles reflect the relative intensities of each formula.

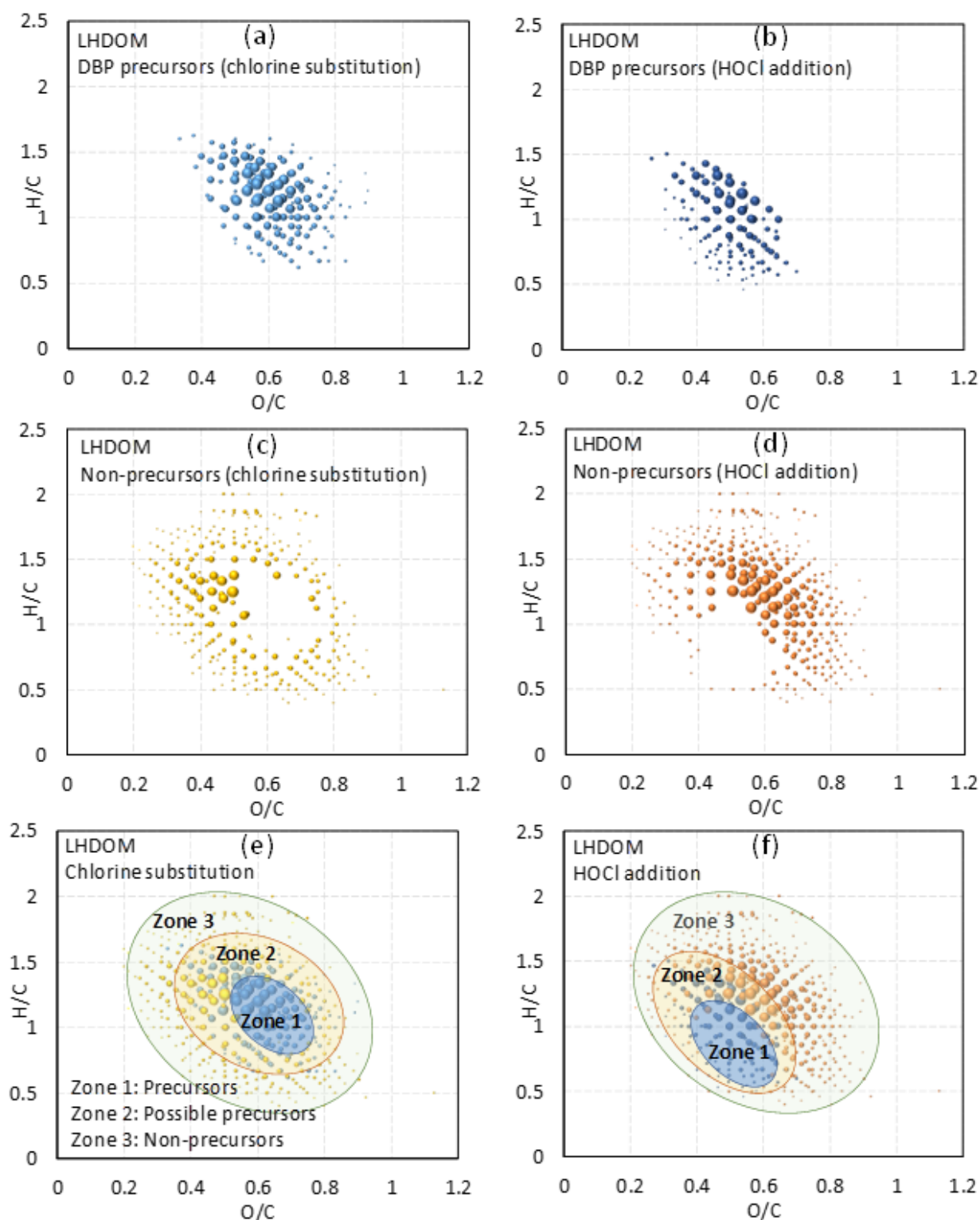


Figure S11. Van Krevelen diagrams of $C_{9-16}H_nO_m$ formulas in LHDOM and LHDOM-AOP. The formulas were classified as (a)–(b) DBP precursors and (c)–(d) non-precursors. Two chlorination pathways, chlorine substitution and HOCl addition, were considered. (e)–(f) The van Krevelen space

was divided into three zones based on the possibility of the $C_{9-16}H_nO_m$ formulas located in each zone to match with their corresponding DBPs. Note that the diagrams only covered $C_{9-16}H_nO_m$ formulas in LHNOM because the carbon number of the DBPs detected mainly ranges from 9–16.

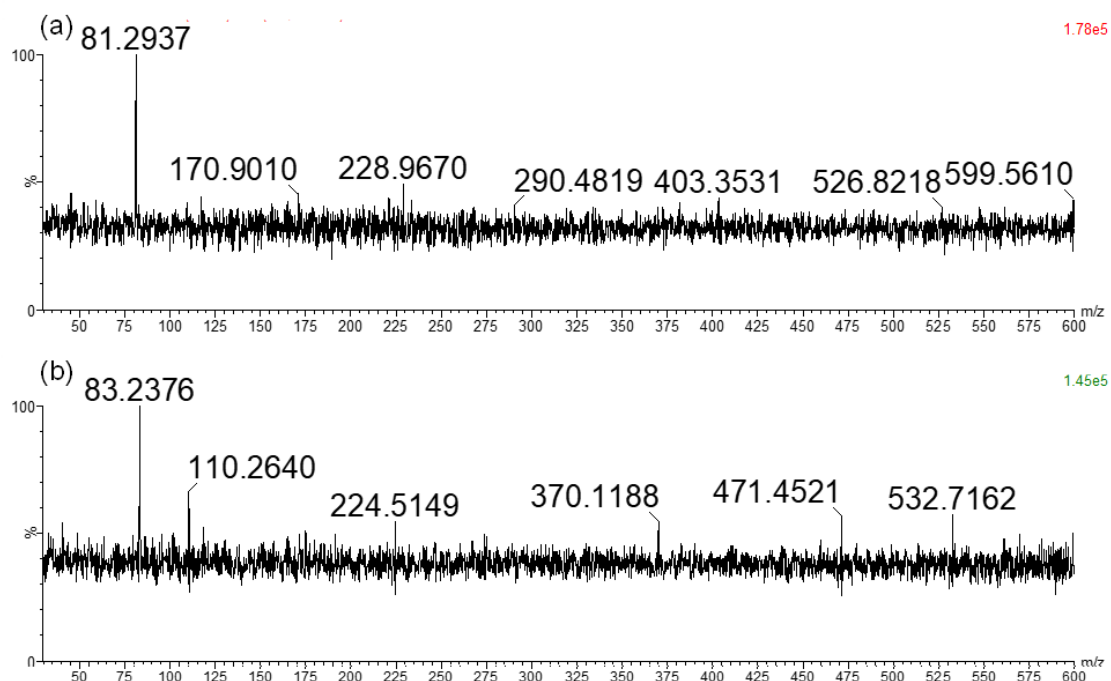


Figure S12. ESI-tqMS precursor ion scan spectra of (a) m/z 35 and (b) m/z 37 of 1,2,4,5-benzenetetracarboxylic acid treated by 3-day chlorination.

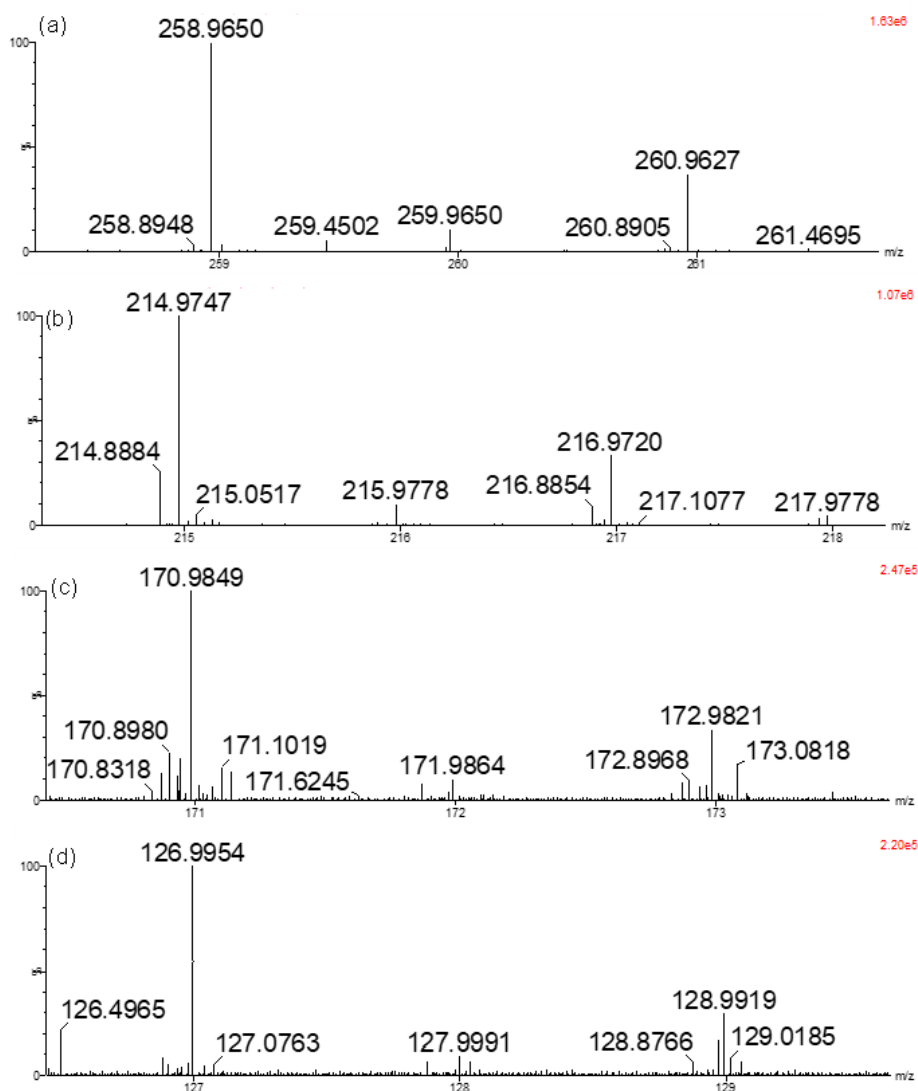


Figure S13. High-resolution mass spectrometry full scan spectra of the chlorine-containing products generated from 1,2,4,5-benzenetetracarboxylic acid treated by the UV/H₂O₂ AOP followed by 3-d chlorination. Isotope peaks of (a) m/z 258.9650 $C_9H_5O_7Cl$; (b) m/z 214.9747 $C_8H_5O_5Cl$; (c) m/z 170.9849 $C_7H_5O_3Cl$; (d) m/z 126.9954 C_6H_5OCl .

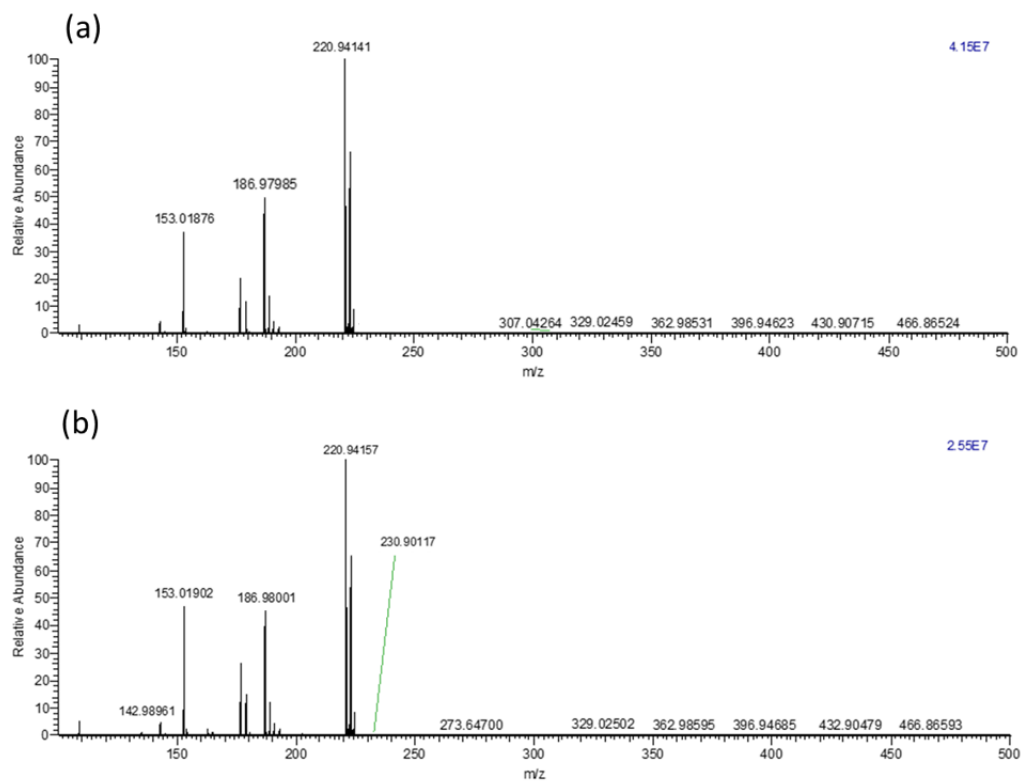


Figure S14. High-resolution mass spectrometry full scan spectra of 2,6-dihydroxybenzoic acid after (a) the 3-d chlorination and (b) the UV/H₂O₂ AOP followed by 3-d chlorination.

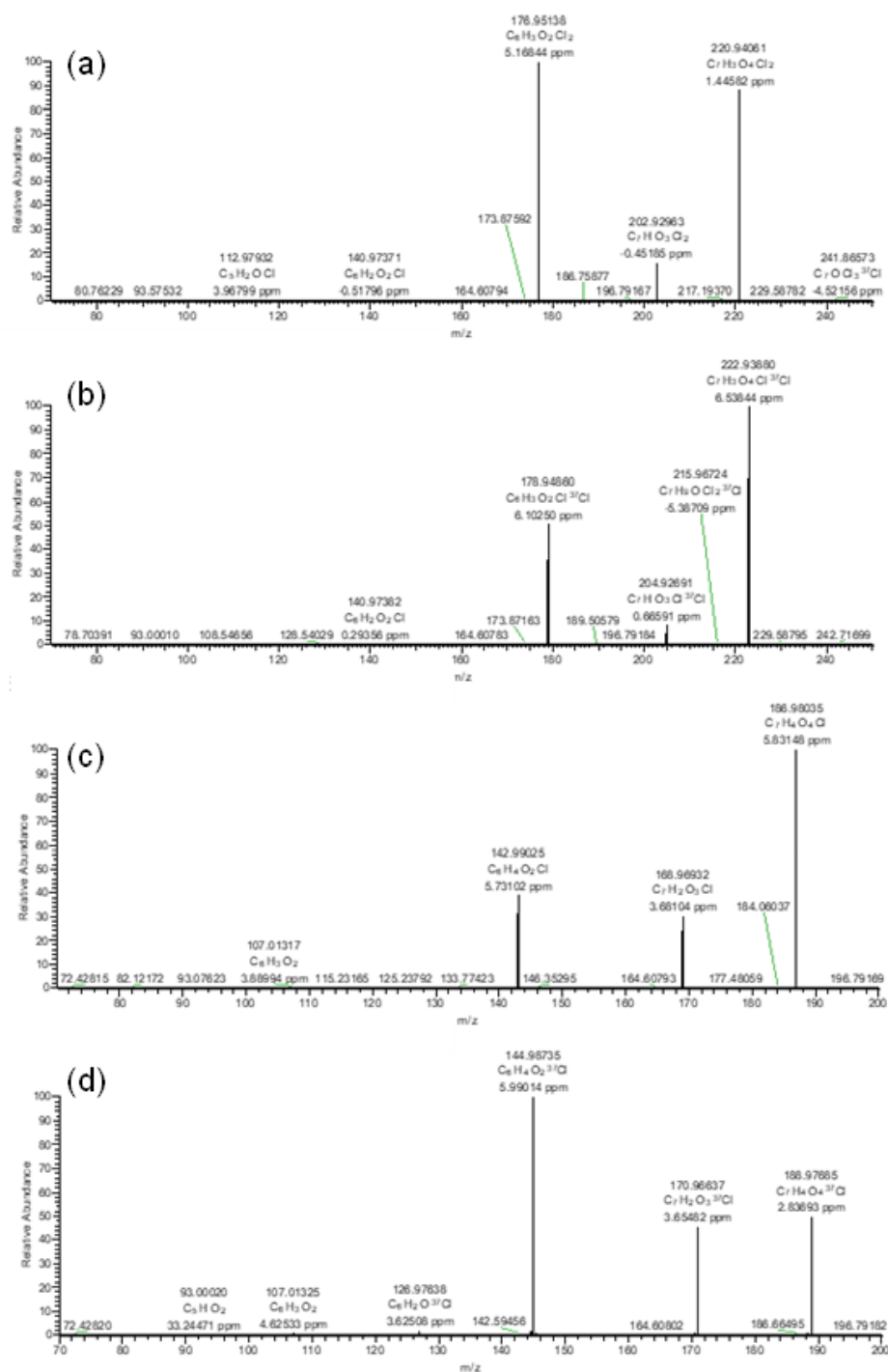


Figure S15. High-resolution mass spectrometry product ion scan spectra of the chlorine-containing products generated from 2,6-dihydroxybenzoic acid treated by the UV/ H_2O_2 AOP followed by 3-d chlorination. Product ion scan spectra of (a) m/z 220.9408 $C_7H_4O_4^{35}Cl_2$; (b) m/z 222.9381 $C_7H_4O_4^{35}Cl^{37}Cl$; (c) m/z 186.9798 $C_7H_5O_4^{35}Cl$ and (d) m/z 188.9769 $C_7H_5O_4^{37}Cl$.

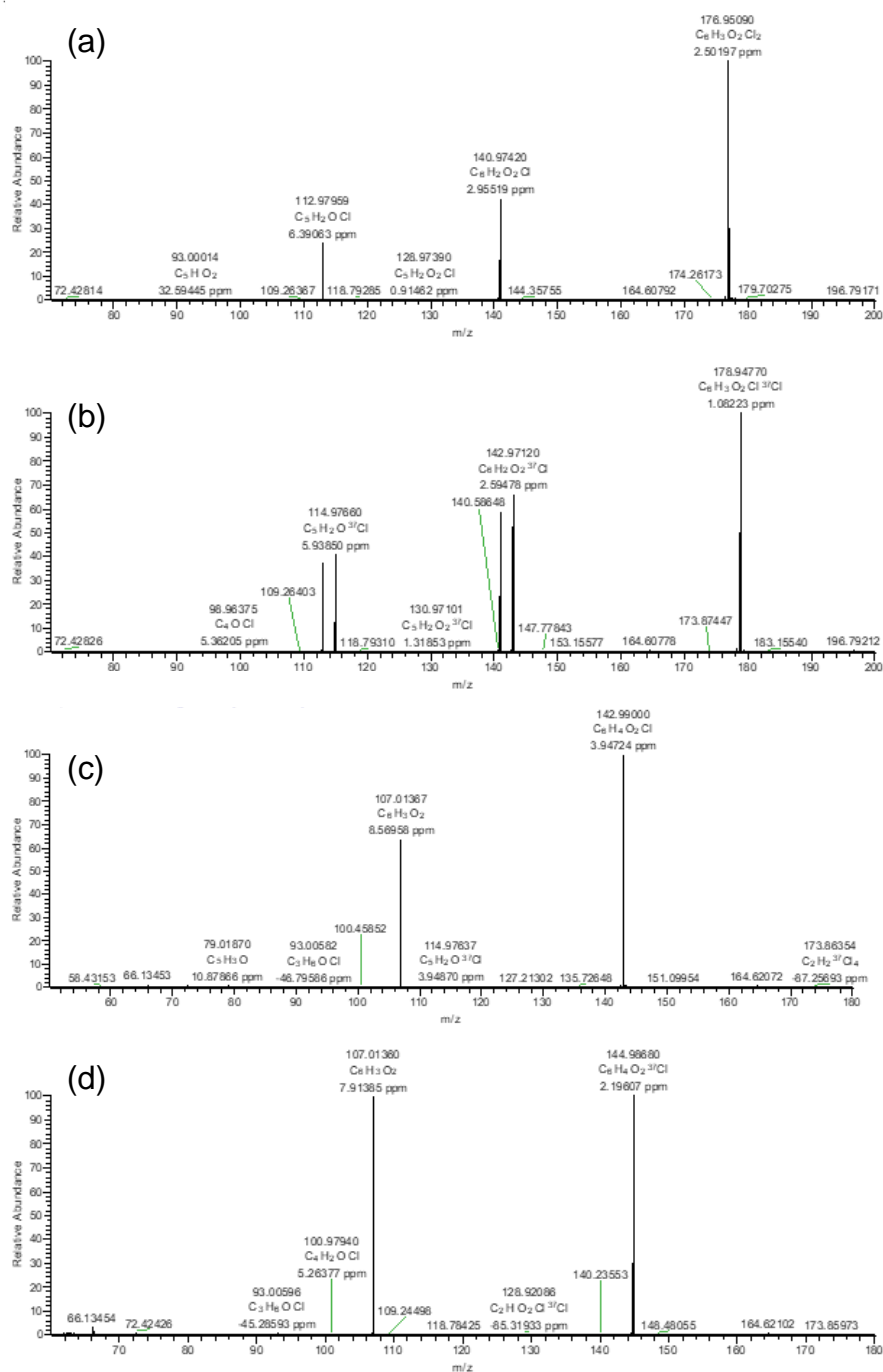


Figure S16. High-resolution mass spectrometry product ion scan spectra of the chlorine-containing products generated from 2,6-dihydroxybenzoic acid treated by the UV/ H_2O_2 AOP followed by 3-d chlorination. (a) m/z 176.9510 $C_6H_4O_2^{35}Cl_2$; (b) m/z 178.9481 $C_6H_4O_2^{35}Cl^{37}Cl$; (c) m/z 142.9900 $C_6H_5O_2^{35}Cl$ and (d) m/z 144.9870 $C_6H_5O_2^{37}Cl$.

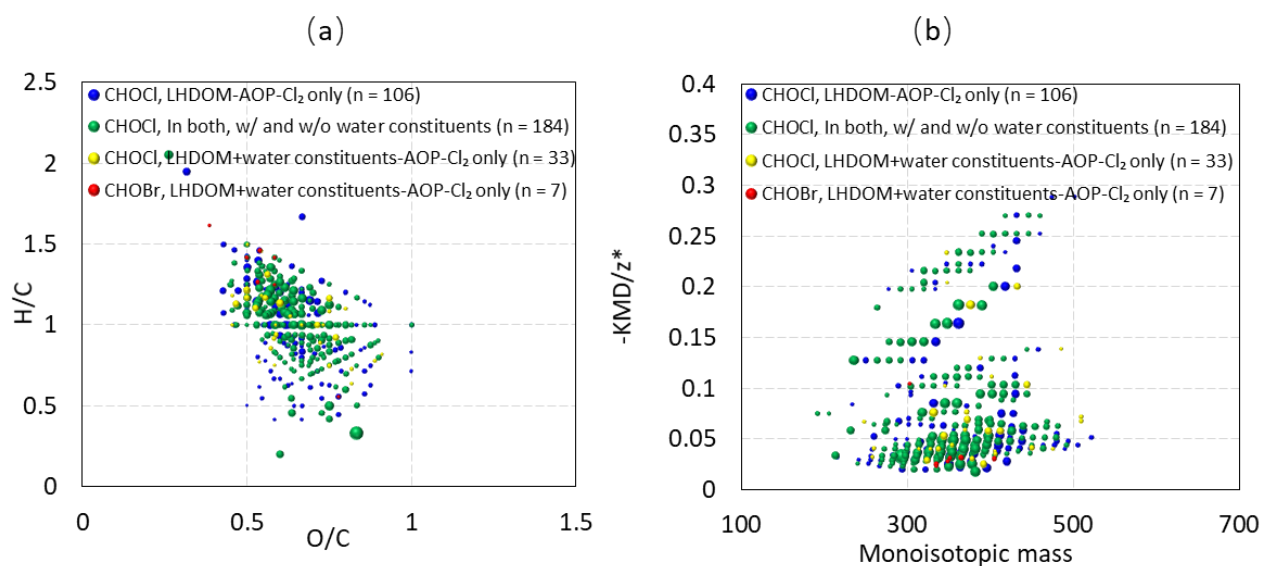


Figure S17. (a) Van Krevelen diagram and (b) modified Kendrick plots of CHOC1 and CHOBr DBPs produced during 3-day chlorination of AOP-treated LHDOM in the presence and in the absence of water constituents.

Table S1 Summary of weighted mean values of O/C, H/C, DBE/C and AI_{mod} of formulas in SRNOM and SRNOM-AOP.

Fraction	O/C _w	H/C _w	DBE/C _w	$AI_{mod,w}$
SRNOM only	0.466	0.957	0.560	0.425
In both (decreased)	0.503	0.887	0.599	0.471
SRNOM AOP only	0.603	0.996	0.541	0.342
In both (increased)	0.669	1.119	0.500	0.250

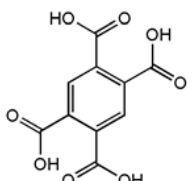
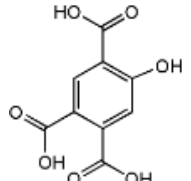
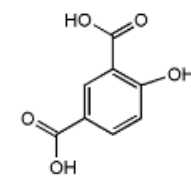
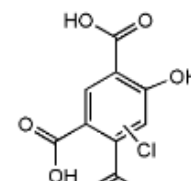
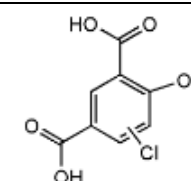
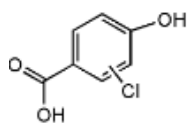
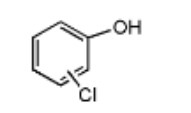
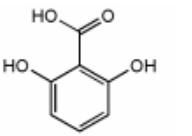
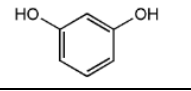
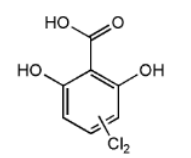
Table S2 Number and ratio of DBPs that can find the precursors in SRNOM vs. SRNOM-AOP
(C₇₋₂₂ represents the range of the carbon number of DBPs)

Sample	Total number of C ₇₋₂₂ -DBPs after 3-day chlorination	C ₇₋₂₂ -DBPs that can find precursors (chlorine substitution)		C ₇₋₂₂ -DBPs that can find precursors (HOCl addition)	
		Number	Ratio	Number	Ratio
SRNOM	1320	1056	80%	792	60%
SRNOM-AOP	1361	1170	86%	898	66%

Table S3 Summary of weighted mean values of O/C, H/C, DBE/C and AI_{mod} of formulas in LHDOM and LHDOM-AOP.

Fraction	O/C _w	H/C _w	DBE/C _w	AI _{mod,w}
LHDOM only	0.473	1.179	0.461	0.294
In both (decreased)	0.357	1.219	0.444	0.326
LHDOM AOP only	0.532	1.193	0.447	0.250
In both (increased)	0.645	1.235	0.444	0.182

Table S4 List of products detected by high-resolution mass spectrometry.

Model compound	Elemental formula	Measured m/z	Calculated m/z	Mass error (ppm)	Proposed structure
 $C_{10}H_6O_8$ m/z 252.9989	$C_9H_6O_7$	225.0035	225.0041	2.7	
	$C_8H_6O_5$	181.0138	181.0142	2.21	
	$C_9H_5O_7Cl$	258.9650	258.9651	0.39	
	$C_8H_5O_5Cl$	214.9747	214.9753	2.79	
	$C_7H_5O_3Cl$	170.9849	170.9854	2.92	
	C_6H_5OCl	126.9954	126.9956	1.57	
 $C_7H_6O_4$ m/z 153.0193	$C_6H_6O_2$	109.0293	109.0295	1.83	
	$C_7H_4O_4Cl_2$	220.9447	220.9414	14.94	

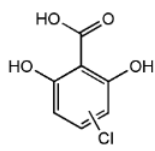
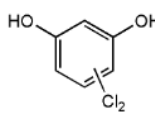
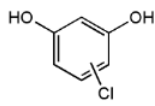
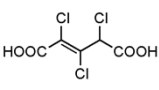
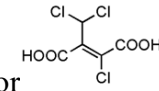
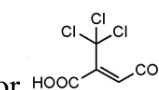
	C ₇ H ₅ O ₄ Cl	186.9797	186.9803	3.21	
	C ₆ H ₄ O ₂ Cl ₂	176.9511	176.9515	2.26	
	C ₆ H ₅ O ₂ Cl	142.9897	142.9905	5.59	
	C ₅ H ₃ O ₄ Cl ₃	230.9010	230.9024	6.06	 or  or 

Table S5 Concentrations of water constituents

HCO ₃ ⁻ (mM)	HNO ₃ ⁻ (mg/L)	SO ₄ ²⁻ (mg/L)	Cl ⁻ (mg/L)	Br ⁻ (μg/L)
1	5	10	10	20

References:

- [1] Gonsior, M.; Zwartjes, M.; Cooper, W.J.; Song, W.; Ishida, K.P.; Tseng, L.Y.; Jeung, M.K.; Rosso, D.; Hertkorn, N.; Schmitt-Kopplin, P. Molecular characterization of effluent organic matter identified by ultrahigh resolution mass spectrometry. *Water Res.* **2011**, *45*, 2943–2953.
- [2] Fang, J.; Fu, Y.; Shang, C. The roles of reactive species in micropollutant degradation in the UV/free chlorine system. *Environ. Sci. Technol.* **2014**, *48*, 1859–1868.